1-2023

Recent Advances in Experimental Design and Data Analysis to Characterize Prokaryotic Motility

Megan M. Dubay
Portland State University, dubaymae@pdx.edu

Jacqueline Acres
Portland State University, acres@pdx.edu

Max Riekeles
Technical University Berlin

Jay Nadeau
Portland State University, jay.nadeau@pdx.edu

Citation Details

Dubay, M. M., Acres, J., Riekeles, M., & Nadeau, J. L. (2022). Recent advances in experimental design and data analysis to characterize prokaryotic motility. Journal of Microbiological Methods, 106658.

Journal of Microbiological Methods 204 (2023) 106658

Contents lists available at ScienceDirect

Journal of Microbiological Methods

journal homepage: www.elsevier.com/locate/jmicmeth

Review

Recent advances in experimental design and data analysis to characterize prokaryotic motility

Megan Marie Dubay [a,1], Jacqueline Acres [a], Max Riekeles [b], Jay L. Nadeau [a,*]

[a] Department of Physics, Portland State University, 1719 SW 10th Ave., Portland, OR 97201, United States of America
[b] Astrobiology Group, Center of Astronomy and Astrophysics, Technical University Berlin, Hardenbergstraße 36A, 10623 Berlin, Germany

ARTICLE INFO

Keywords:
Biological optics
Cell locomotion
Chemotaxis
Biological movement

ABSTRACT

Bacterial motility plays a key role in important cell processes such as chemotaxis and biofilm formation, but is challenging to quantify due to the small size of the individual microorganisms and the complex interplay of biological and physical factors that influence motility phenotypes. Swimming, the first type of motility described in bacteria, still remains largely unquantified. Light microscopy has enabled qualitative characterization of swimming patterns seen in different strains, such as run and tumble, run-reverse-flick, run and slow, stop and coil, and push and pull, which has allowed for elucidation of the underlying physics. However, quantifying these behaviors (e.g., identifying run distances and speeds, turn angles and behavior by surfaces or cell-cell interactions) remains a challenging task. A qualitative and quantitative understanding of bacterial motility is needed to bridge the gap between experimentation, omics analysis, and bacterial motility theory. In this review, we discuss the strengths and limitations of how phase contrast microscopy, fluorescence microscopy, and digital holographic microscopy have been used to quantify bacterial motility. Approaches to automated software analysis, including cell recognition, tracking, and track analysis, are also discussed with a view to providing a guide for experimenters to setting up the appropriate imaging and analysis system for their needs.

1. Introduction

Since the development of a tracking microscope in 1971 (Berg, 1971), researchers have recognized the need for tools that would allow for both imaging and recording of microbial motility. The ideal experimental apparatus would record images of cells in a 3D volume with high signal to noise ratios and at high framerates. This would in turn allow cell tracking algorithms to easily characterize cell motility quickly and effectively, preferably with minimal user input. Advances over the past few decades have brought this ideal case closer to reality. Unfortunately, despite numerous experimental setups and data analysis techniques, the holy grail of precise and straightforward 3D tracking of bacteria remains elusive. That being said, progress has been made in understanding motility phenotypes of various bacteria using a variety of imaging and software techniques, which we will summarize here with the goal of making it easier for those planning bacterial tracking experiments to choose hardware and software.

Acquisition and analysis software may be open-source or commercial. Choices are determined by the project's budget as well as any needs to re-tune available code to custom optical systems. The platforms ImageJ (FIJI) (Schindelin et al., 2012) and ICY (de Chaumont et al., 2012) are highly versatile, open source, and widely used by biologists, so in this review we will mention when a FIJI or ICY package or plug-in exists for a particular technique. Many packages for MATLAB are also available, as well as custom programs based in Python.

Several recent reviews of cell and particle motility exist, and we will focus on areas complementary to those recently discussed. One thorough review covers tracking of more complex cells, which largely applies to 2D processes such as cell migration as well as tracking of sub-cellular organelles, and offers a comprehensive list of software for this application (Emami et al., 2021). While there is significant overlap with bacterial tracking, the latter presents certain specific challenges, particularly fast speeds and 3D motion. It is also simpler in some respects, since contouring is usually not necessary and subcellular features are neglected. Another recent review focuses on ameboid motility to illustrate the steps required in motility quantification of complex cells (Boquet-Pujadas et al., 2021). Single-molecule investigations of bacterial cells using high resolution fluorescence techniques have been also

* Corresponding author at: SRTC Room 134, Department of Physics, Portland State University, 1719 SW 10th Ave., Portland, OR 97201, United States of America.
E-mail address: nadeau@pdx.edu (J.L. Nadeau).
[1] Current address: Department of Physics and Astronomy, University of North Carolina, 120 E. Cameron Ave., Chapel Hill, NC 27514, United States of America.

https://doi.org/10.1016/j.mimet.2022.106658
Received 7 November 2022; Received in revised form 13 December 2022; Accepted 13 December 2022
Available online 15 December 2022

well reviewed elsewhere (Gahlmann and Moerner, 2014). Additionally, "microswimmers" may also refer to non-living particles. Many studies have been conducted on microspheres (Lee et al., 2007a; Lei et al., 2015; Zhang et al., 2017) and other types of nonliving swimmers, and approaches to their tracking have been reviewed (Pané et al., 2019). Although nonliving particles can be used to approximate bacteria in size, their lack of self-motility and relatively slow speeds simplify data processing in ways that are not possible for bacteria; in addition, they may be engineered to provide contrast for different imaging techniques. We will limit the scope of the current review to tracking of unstained, self-motile microorganisms on the order of 1–2 μm in diameter and the unique challenges these present, specifically complex, frequently overlapping tracks and speeds of up to hundreds of cell lengths per second.

1.1. Bacterial motility

Motility is a crucial microbial phenotype that has evolved independently in Bacteria, Eukarya, and Archaea. On the molecular level, 18 different motility types can currently be identified, with more undoubtedly to be discovered in microorganisms that have not yet been cultured (Miyata et al., 2020). Some bacteria use flagella for swimming motility, whereas archaea use the unrelated archaellum (Albers et al., 2018; Albers and Jarrell, 2015). Directional motion allows microorganisms to find nutrients, escape predators, waste products, and toxins, and assemble into biofilms. The best studied microorganisms are *Escherichia coli* (*E. coli*) and *Salmonella enterica* serovar Typhimurium, and much of what we know about motility and chemotaxis come from these organisms (Bardy et al., 2017).

Research into different microorganisms with different motility patterns has grown over the past two decades, identifying new classes of motility, motility in new classes of microorganisms, and elucidating the physics of swimming at the micron scale. Flagellins are highly conserved in bacteria, but flagellar conformations of bacteria and archaea vary greatly, as do body shapes, as shown in Fig. 1 (a), (b). At least six types of swimming patterns can be distinguished in low-resolution microscopic recordings; these correspond to both flagellar arrangement and function. The common gut and soil bacteria *Escherichia coli* and *Bacillus subtilis* have peritrichous flagella and show a well-characterized pattern of motility involving "runs" (where all the flagella rotate together in a bundle, turning counter-clockwise) and "tumbles" (where the flagella turn clockwise and the bundle separates) (Fig. 1 (c)). Bacteria with peritrichous flagella that only rotate clockwise can show run-and-stop or run-and-slow patterns (Armitage and Schmitt, 1997) (Fig. 1 (d)). Another pattern, the "run-reverse flick" pattern of aquatic microorganisms with a single polar flagellum, such as *Vibrio alginolyticus*, is also known (Fig. 1 (e)) (Stocker, 2011a). This pattern of swimming, common in marine bacteria, involves 180-degree reversals, creating zig-zag tracks, often at high speeds compared to bacteria with peritrichous flagella (up to 100 μm/s vs. 10–30 μm/s). Another type of swimming seen with a single flagellum is the stop-and-coil motion of microorganisms such as *Rhodobacter sphaeroides*, where the flagellum cannot reverse direction, so it coils in order to allow the microorganism to change orientation (Armitage, 1999) (Fig. 1 (f)). Motile magnetotactic cocci have been identified that have peritrichous flagella and swim in a helical motion due to push-pull action of the flagella (Zhang et al., 2014) (Bente et al., 2020) (Fig. 1 (g)). Swimming patterns of spiral-shaped cells are characterized more by the appearance of the cells themselves rather than the track of movement. In Spirochetes such as *Borrelia* and *Treponema*, pairs of flagella rotate within the periplasm, generating a helical wave (Tahara et al., 2018). In spirochaetes, two "run" modes and two non-translational modes have been identified. In general, changes in flagellar number, arrangement, hook length, or other parameters profoundly (Zhu et al., 2022) affect motility and chemotaxis patterns (Najafi et al., 2018).

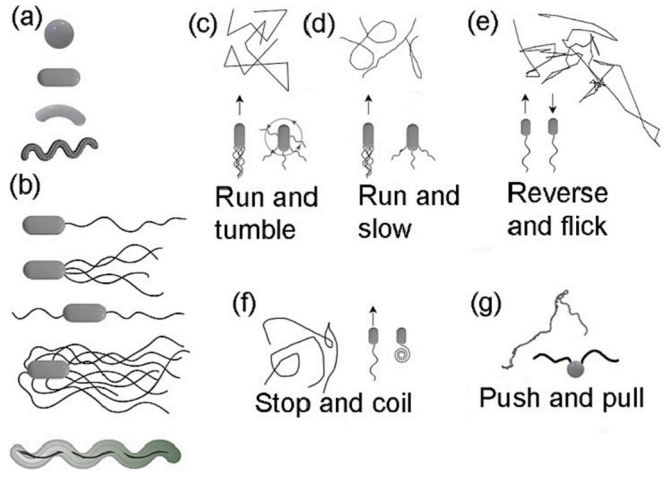

Fig. 1. Cell morphologies and swimming patterns. (a) Both bacteria and archaea show a variety of body shapes that can be classified as cocci (spherical), bacilli (rods), curved rods, or spirals. (b) Flagella and archaella may be attached to the cell in a variety of patterns. A rod-shaped body is shown for simplicity, but the different flagellar patterns are seen across body types. From top to bottom are monotrichous (a single flagellum, which may be lateral or polar), lophotrichous (multiple flagella attached at a single point), amphitrichous (flagella on each end), peritrichous (multiple flagella attached at different points all over the surface), and periplasmic (flagella enclosed in the periplasmic space). (c) Run-and tumble pattern as exemplified by *E. coli*. (d) Run-and slow pattern as exemplified by *Sinorhizobium melioti*. (e) Reverse and flick as exemplified by *V. alginolyticus*. (f) Stop and coil as exemplified by *R. sphaeroides*. (g) Push and pull as identified by the eukaryote *Chlamydomonas*.

Other types of swimming continue to be elucidated. *Synechococcus* is a cyanobacterium that swims without flagella (Waterbury et al., 1985). Other types of non-swimming motility are also seen but are less understood. Type IV pili are used by many species for motility on surfaces, usually called twitching motility (Piepenbrink et al., 2016). Gliding refers to a surface mechanism used by a heterogeneous group of bacteria, powered by ion channels and secretory mechanisms independent of flagella (Nan and Zusman, 2016). Sliding is a type of surface motility that requires no active motor (Holscher, 2017). Staphylococci, previously considered non-motile, have been shown to have means of locomotion that include spreading, darting, and comet formation (Pollitt and Diggle, 2017). In this review we focus on motility that is tracked in liquid medium, thus restricting our discussion to swimming and to some extent gliding.

Much less is known about swimming in archaea, although it has been known for some time that swimming is induced by rotation of the archaellum. Much of the difficulty in studying these microorganisms arises from the need to observe them under extremophilic conditions: anaerobic, temperature extremes, and/or very high salt. A systematic study of the swimming patterns of several types of archaea was performed in 2012 (Herzog and Wirth, 2012a). Some archaea show the fastest movement relative to body size of any known organism on Earth. The patterns of fast-swimming archaea were characterized as "run and seek," with different behaviors (slower zig-zagging) near the surface of the slide. The tracks are closest to the bacterial "run and flick" pattern, but many archaea are distinguished by their remarkable speeds. Some microscopy systems designed to accommodate the needs of archaea will be specifically mentioned in this paper.

High-resolution recordings permit observation of detailed features of tracks rather than characterizing all forward motion as simply "runs." These studies have led to an increasing appreciation of the importance of cell body shape in swimming. The cell body is often considered to be a source of passive drag, but non-rod-shaped cell bodies may contribute to motility. Many marine motile bacteria are curved rods falling within a relatively narrow range of elongation and curvature. Detailed models of swimming speeds and chemotaxis efficiencies have identified shapes that are optimized across a panel of selective parameters (Schuech et al.,

2019). Even more recently, helical motion of a crescent-scaped bacterial cell, *Caulobacter crescentus*, was observed to affect swimming patterns in this singly flagellated cell (Yuan et al., 2021).

1.2. Imaging challenges

Understanding motility phenotypes provides a framework of what quantities might be of interest to characterize and quantify bacterial motility. For instance, the length of a bacterium's "run" could change based on environmental factors such as viscosity. Rapid characterization of run length for numerous cells would give good statistics and provide a sound basis of comparison. However, quantification of bacterial motility remains challenging due to the technological difficulty of imaging live, active microorganisms on the order of the size of 2λ of visible light that can move tens or even hundreds of cell lengths per second. For any imaging system, a variety of trade-offs must be made according to the specific goals of the experiment. Increased spatial resolution usually leads to decreased field of view, unless cameras with very high sensor sizes are used. High frame rates are necessary to capture fast processes but lead to extremely large datasets if carried out over long times. Fluorescent labels increase signal to noise of imaging, but dyes may affect microorganism behavior. Finally, data may be analyzed cell by cell, which optimizes accuracy but limits the number of cells considered; or statistical analyses may treat hundreds to thousands of cells at a time but fall prey to false positive and false negative identification of tracks.

The purpose of this review is to identify the recent breakthroughs in bacterial motility analysis and identify what parameters of an imaging system are necessary to study the identified phenomena and what the limiting technological factors are in each case. Summary tables are provided that should assist researchers in choosing imaging and tracking techniques that are appropriate for the systems studied, or in developing custom systems that can push the limits of what is currently known. Both hardware and software are considered, with particular attention to automated identification and tracking algorithms.

2. Microscopy techniques

Throughout the years, a variety of imaging techniques have been employed with the goal of bacterial tracking. These include phase contrast microscopy, darkfield microscopy, fluorescence microscopy, and digital holographic microscopy (both in-line and off-axis). Each system has tradeoffs; the most commonly used in recent studies are discussed in detail below.

2.1. Phase contrast microscopy

Phase contrast microscopy is a standard technique found in most microbiology laboratories and easily implemented on all commercial microscopes. Depending upon the objective lens chosen, it is capable of either high resolution or fairly large depth of field. Diffraction-limited lateral (XY) resolution is given by λ/NA, where λ is the wavelength of illuminating light and NA is the numerical aperture of the objective. Depth of field *d* is the sum of two terms, a wave term and a geometrical optical term (Davidson and Spring, n.d.):

$$d = \frac{n\lambda}{(NA)^2} + \frac{ne}{M(NA)} \quad (1)$$

where *n* is index of refraction of the medium between the lens and the coverslip (air or immersion oil), *e* is the smallest resolvable element, and *M* is the magnification. (Fig. 2).

Phase contrast microscopy represents one of the most established and successful methods of bacterial tracking. It has been used for some significant recent results, such as tracking a variety of swimming archaea, including hyperthermophiles (Herzog and Wirth, 2012b) and discovery of the importance of cell body motion in swimming of

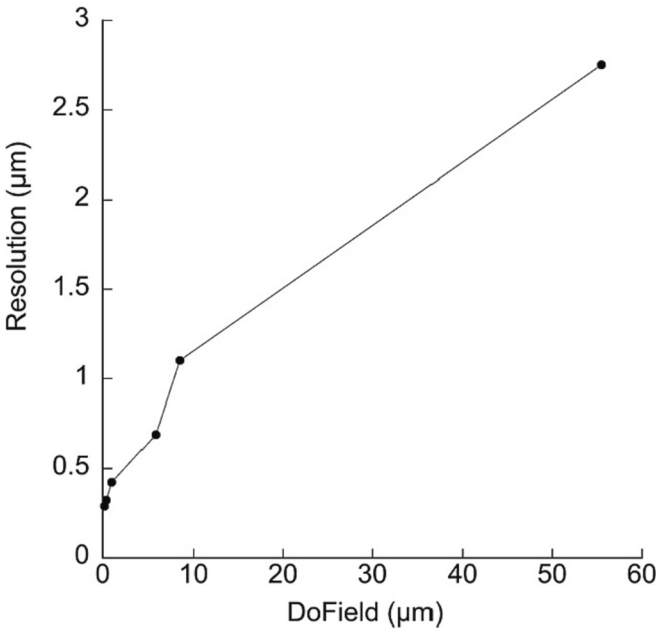

Fig. 2. Tradeoff between resolution and depth of field for 550 nm illumination and air objectives. The non-linear relationship can be appreciated by observing that for bacterial cells on the order of 1 μm, the ability to resolve the cells will lead to a depth of field of <10 μm, whereas a decrease of resolution for 2.5 μm will permit a depth of field of >50 μm.

Caulobacter (Liu et al., 2014).

The primary disadvantage of phase contrast microscopy is that cells are lost as they swim in X and Y, or out of focus in the Z plane. Manual manipulation or digital tracking stages may be used to follow cells. Methods to follow single cells include the use of scanning stages (Berg and Brown, 1974; Frymier et al., 1995; Yang et al., 2015) or scanning objectives (Corkidi et al., 2008). These methods are limited by their scanning speed. Most recently, a technique has been proposed for determining Z depth in out-of-focus microorganisms by fitting the Airy ring pattern to calibrated patterns from test cells (Taute et al., 2015).

In some experiments, it is not necessary to permit the cells to swim freely in Z. In this case, sample chambers or flow cells may be constructed that restrict the cells to a single focal plane. This is useful when only 2D motion is necessary, such as to determine the fraction of motile cells or a general idea of the swimming speed. This may be useful for determining cell health or growth phase (Ziegler et al., 2015).

The typical light microscopes used for phase contrast (or related techniques such as differential interfererence contrast [DIC]) may be modified for use with extremophiles. The low-temperature swimming record seen in the bacterium *Colwellia psychrerythrea*, −15 °C, was determined using a laboratory microscope customized by the vendor for use at subzero temperatures. The entire instrument and its operator were then located in an adjustable-temperature cold room (Junge et al., 2003). At the other extreme, a heated indium tin oxide (ITO) chamber heated to 75 °C, with the microscope objectives heated to 65 °C, was used for imaging hyperthermophilic archaea (Charles-Orszag et al., 2021).

2.2. Digital holographic microscopy

Digital holographic microscopy (DHM) is a volumetric technique based upon interferometry, where a volume of view is captured in a single snapshot (hologram). The hologram appears as a pattern of Airy rings indicating out-of-focus objects throughout the focal depth. The typical approach to analyzing DHM data is to reconstruct the optical field through a chosen Z depth and spacing based upon the hologram.

Reconstruction methods depend upon the DHM geometry used, namely "off-axis", where object and reference beams interfere at an angle (Fig. 3 (a)), or "inline" imaging (DIHM) where a single beam serves as both object and reference (Fig. 3 (b)). The different approaches to geometry and reconstruction have been reviewed in (Xiao et al., 2014) and (Myung, 2010).

Off-axis holography separates the spatial frequencies from the unscattered "direct term" as well as separating the real and virtual images from one another, facilitating ease of reconstruction into both amplitude and quantitative phase images (Schnars and Jüptner, 2002). Amplitude images are equivalent to transmission light microscopy. Quantitative phase images have no direct counterpart in ordinary light microscopy and are related to the product of the cell thickness h and the difference in refractive index between the medium (n_m) and cell (n_c), with the phase shift $\Delta\phi$ given by (Marquet et al., 2005; Rappaz et al., 2005) (Marquet et al., 2005).

$$\Delta\phi = \frac{2\pi}{\lambda} h(n_c - n_m) \tag{2}$$

where λ is the wavelength of illumination. This value is modulo 2π, so complications arise when $\Delta\phi$ exceeds 2π. However, for experiments involving bacteria, this is rarely an issue. Instead, the challenge lies in resolving any phase shift, as $n_c - n_m$ is on the order of 0.03–0.05 (Wyatt, 1970), and methods such as frame averaging to reduce noise cannot be performed on rapidly moving cells.

The lateral resolution of DHM is equivalent to that of brightfield microscopy. Reconstruction of DIHM images is more complicated, since the direct term is not readily filtered out, leading to "ghost" images. Nonetheless, many algorithms have been developed for reconstruction and phase retrieval from these images (Galande et al., 2021; Latychevskaia and Fink, 2009; Micó et al., 2011; Wang et al., 2018; Zhang et al., 2003).

The limit to the depth that can be reconstructed from DHM results from a degradation of spatial resolution as the reconstruction propagator extends outside the focal plane. For typical bacterial imaging experiments with ~1 μm spatial resolution, the depth of the sample is limited to ~1 mm (Kühn et al., 2014), which is very large compared with other microscopic techniques and which represents the biggest advantage of this imaging technique, allowing a simultaneous snapshot of essentially an unconstrained volume. Acquisition rates are limited by the camera frame rate. As a result of this major advantage, a large number of recent papers have reported prokaryotic tracking using DHM. The optics of DHM are also simple and the hardware is low in cost.

The disadvantage of DHM is a generally low resolution (Peng and Caojin, 2022), and the intrinsic low contrast of most prokaryotic cells in amplitude and phase. Some dyes may increase contrast for DHM, but this is an area that has not been well explored (Nadeau et al., 2016). The development of agents for specific enhancement of phase contrast has also been little studied, though it is possible through labeling techniques such as genetically encoded air-filled vesicles which provide substantial change in refractive index relative to aqueous medium (Farhadi et al., 2020).

DHM leads to large datasets and its analysis is computationally intensive. A 30 s dataset at 15 frames/s and 4 Mpx yields 1.8 GB of images before reconstruction. Depending upon the z-spacing selected for reconstruction, a full reconstructed dataset may be upwards of 1 Tb. Few software packages are available for analysis. Commercial software is usually tied to a specific instrument. Open-source Fiji for both in-line and off-axis DHM have recently been reported (Buitrago-Duque and Garcia-Sucerquia, 2022) (Cohoe et al., 2019).

An alternative to reconstruction is to extract Z information directly from the holograms. If the form of the diffraction pattern or the Z-

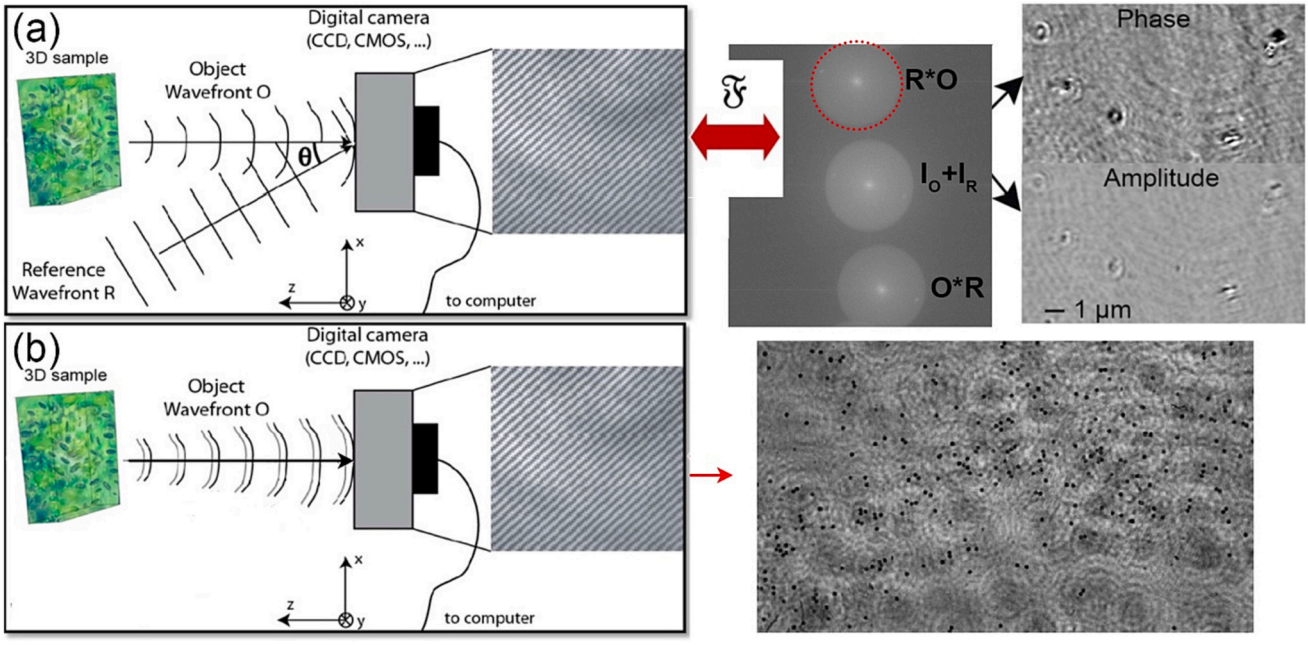

Fig. 3. Off-axis DHM and DIHM. (a) Off-axis holography uses the interference of two coherent beams of light from a single source to record the complete sample volume in each captured frame. The "object" beam passes through the sample, while the "reference" beam takes an identical-length unperturbed path to the detector. The two beams are interfered at the detector array and the resulting interference pattern records a pattern of interference fringes which, in Fourier space, yield the real image (O*R), the virtual image (R*O), and the so-called "direct" term $I_O + I_R$. Either the real or virtual image is selected in Fourier space (as indicated by the red circle) and reconstructed using a chosen algorithm; numerical refocusing allows reconstruction of phase and amplitude images through the depth of the sample. (b) Digital in-line holographic microscopy (DIHM) uses a single beam which is assumed to be slightly perturbed by the object and interferes with itself. The resulting hologram does not capture information as fringes. The illustrated reconstruction method shows a dark-field-like reconstruction that works for phase, amplitude, and phase-amplitude objects (hologram and reconstruction are adapted from (https://www.sciencedirect.com/science/article/pii/S0143816620300762) under terms of the Creative Commons license; the images were cropped). (For interpretation of the references to colour in this figure legend, the reader is referred to the web version of this article.)

position of the object are known, the Airy pattern may be easily fit to a function based upon Lorenz-Mie theory (Cheong et al., 2009; Lee et al., 2007b; Ruffner et al., 2018). For more complex shapes, a discrete dipole approximation must be used (Wang et al., 2014). Open-source software is available to perform these fits, but this approach is highly complex and computationally intensive when neither the exact shape and size nor the axial depth are known. Good signal to noise is also essential to permit accurate fitting of the patterns. This approach has been used to track runs and tumbles in *E. coli* (Wang et al., 2016) (Fig. 4).

DHM instruments are simple and robust and readily adapted to imaging at cold temperatures. We have performed in situ recordings at air temperatures down to −13 °C (Lindensmith et al., 2016). For imaging thermophiles, we have created a low-cost system where the microscope is submerged in a pot of boiling water with the optics protected by a plastic bag. Imaging temperatures of >90 °C can be obtained using this setup (Dubay et al., 2022).

A summary of the hardware and software parameters in recent DHM studies of bacteria is given in Table 1.

2.3. Fluorescence microscopy

Fluorescence microscopy has the highest signal-to-noise of any of the discussed microscopic techniques. It has a higher effective resolution than other techniques because of reduced noise as well as the ability of targeted probes to highlight small structures, such as flagella, that are ordinarily below the diffraction limit. What we mean by "effective resolution" is that the centroid of a high signal-to-noise image can be localized to nanometer precision even if the object's size appears inaccurate. This phenomenon has been used to image individual fluorescent nanoparticles <5 nm in diameter as well as to develop superresolution techniques such as PALM and STORM, where centroids of different objects are separated temporally (Waters and Wittmann, 2014).

While some dyes might affect motility (Martin and Logsdon, 1987; Wainwright et al., 1997), the advantages of fluorescence make it essential whenever high resolution or high signal-to-noise are needed. Membrane dyes have been shown to have less effect on motility and cell division than DNA-targeting dyes (Charles-Orszag et al., 2021). When studying extremophiles, it is important to note that many commonly used dyes do not fluoresce under extremes of temperature, salt concentration, and/or pH, and that cell-wall or membrane-targeting dyes that work in bacteria may not work in archaea. Fluorescent probes that work in thermophiles, halophiles, and at pH extremes have been reported (Leuko et al., 2004) (Rastadter et al., 2022) (Maslov et al., 2018).

At the whole-cell level, the ability to genetically modify bacteria to express fluorescent proteins (FPs) such as green fluorescent protein (GFP) and its variants has enabled numerous tracking experiments in both simple and complex milieux. FPs have little effect on physiology and demonstrate low phototoxicity, permitting them to be used for long-term recordings, although care should be taken to use green light rather than blue or violet for excitation, as the shorter wavelengths affect cell growth (El Najjar et al., 2020). Green excitation corresponds to Yellow Fluorescent Protein (YFP) emission; YFP is very commonly used in microbial studies. The GFP family of proteins requires oxygen for maturation and thus cannot be used in anaerobes; a variety of oxygen-independent alternatives have emerged recently (Chia et al., 2019; Chia et al., 2020; Ko et al., 2020).

For observation of flagella, fluorescence microscopy with labeling is essential. Fluorescence has been used to observe correlate flagellar movements with tumbles in *E. coli, B. subtilis*, and motile *Enterococcus* (Turner et al., 2016). Cells were labeled with the dye Alexa Fluor 532, and an overlay of phase contrast and fluorescence was used to visualize the cell bodies and flagella (Fig. 5 (a)). Fluorescent labeling of flagella may also be used to provide complementary information for cells tracked by other means. One study examining the distribution of

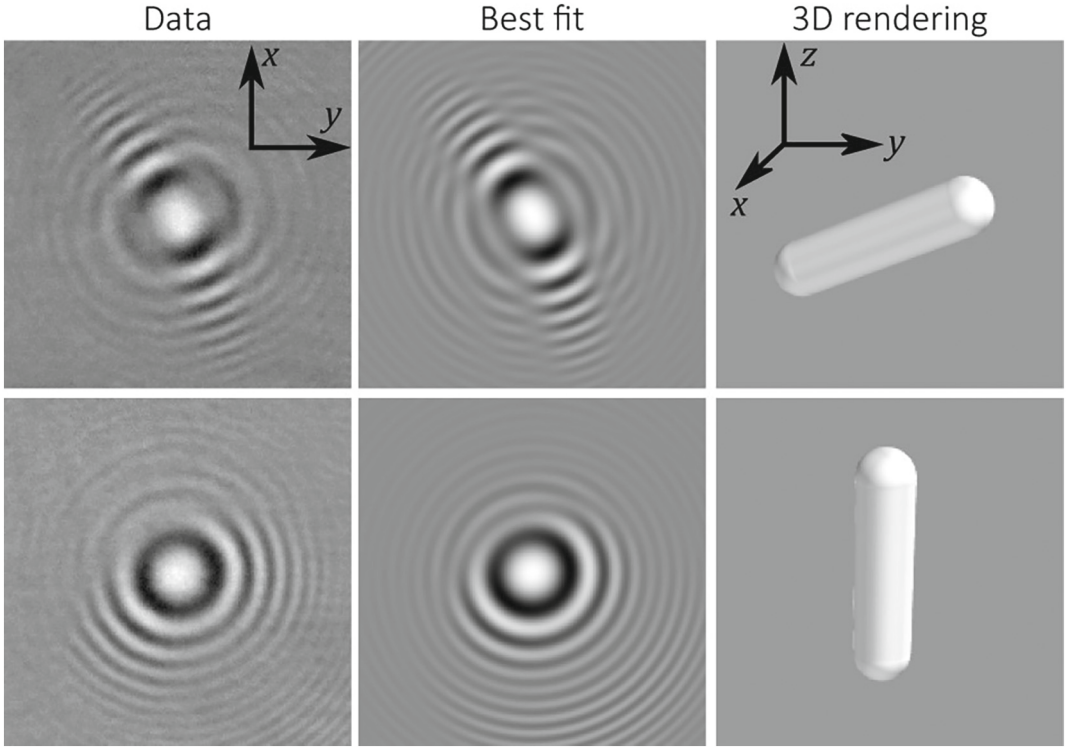

Fig. 4. Holograms of freely swimming *E. coli* in a time series. Two frames are shown in the left column, where the asymmetry in the fringes is noticeably different between the frames. The best-fit holograms are shown in the middle, and three-dimensional renderings from the best-fit holograms are shown on the right using the discrete dipole approximation and the software HoloPy (http://manoharan.seas.harvard.edu/holopy/). (Image from: Anna Wang, Rees F. Garmann, Vinothan N. Manoharan, "Tracking runs and tumbles with scattering solutions and digital holographic microscopy," Opt. Express 24, 23,719–23,725 (2016); © 2016 Optica Publishing Group under the terms of the Open Access license. Image not edited).

Table 1
Imaging parameters in recent bacterial motility studies using holographic microscopy.

Microorganism studied	Software	Objective (s)	λ (nm)	Camera
E. coli[a]	HoloPy	60× NA = 1.2 In-line	660	Photon Focus MVD-1024E-160, 100fps
E. coli[b]	Trajectories linked by home-made Python code	40× NA = 0.6 In-line	455	sCMOS 20 Hz for 2 min
S. marcescens[c]	Manual Tracking / 2D WTMM segmentation method	NA = 0.3 Off-axis	405	170 ms intervals for 3 min
E. coli[d]	No tracking	40× NA = 0.6 100× NA = 1.4 In-line	455 450	sCMOS
E. coli Pseudomonas[e]	Coordinates from Rayleigh-Sommerfeld propagation/ Trajectories from homemade program	40× NA = 0.6 In-line	455	sCMOS 20fps
P. aeruginosa[f]	Bacterial trajectory: bespoke Matlab scripts: DHMTracking and StackMaster	60× NA = 1.4 In-line	685	CMOS 41.6 Hz
E. coli[g]	Image recognition 3D tracking method	40× NA = 0.6 In-line	505	sCMOS 50fps/2 min
E. coli[h]	Median division followed by reconstruction; projection and tracking in XY and manual extraction of Z	20× NA = 0.5	515 642	Mikrotron MC-1362 CMOS 50 fps
Pseudomonas aeruginosa[i]	Median subtraction; reconstruction and projection into XY, XZ, and YZ; polynomial regression smoothing	20× NA 0.4 In-line	532	pco.imaging CMOS 5 fps
B. subtilis[j]	Custom open source reconstruction and tracking software	NA 0.3 aspheres	405	Allied Prosilica GT 15 fps

[a] Wang et al. Optics Express 2016, 24, (21), 23,719–23,725.
[b] Qi et al. Langmuir 2017, 33, (14), 3525–3533.
[c] Marin et al. Methods 2018, 136, 60–65.
[d] Huang et al. Optics Express 2018, 26, (8), 9920–9930.
[e] Peng et al. Langmuir 2019, 35, (37), 12,257–12,263.
[f] Hook, et al. Msystems 2019, 4, (5).
[g] Wang et al. Optics Express 2020, 28, (19), 28,060–28,071.
[h] Farthing et al. Optics Express 2017, 25, (23), 28,489–28,500.
[i] Vater et al. PLoS One 2014, 9, (1), e87765.
[j] Dubay et al. Frontiers in Microbiology 2022 https://doi.org/10.3389/fmicb.2022.836808

flagellar filaments FlaA and FlaB used fluorescent labeling of inserted cysteine residues to visualize the flagella in individual cells, then used DHM without labeling for high-throughput tracking (Fig. 5 (b)) (Kuhn et al., 2018).

The biggest drawback for long-term fluorescence microscopy is photobleaching. Photobleaching may be reduced by limiting light intensity and/or exposure times or by the addition of antioxidants to the medium (or the removal of oxygen if possible) (Bernas et al., 2004; Boudreau et al., 2016; Giloh and Sedat, 1982).

Parameters of recent bacterial tracking studies using fluorescence microscopy are summarized in Table 2.

2.4. Differential dynamic microscopy

Differential dynamic microscopy (DDM) is a recent method (introduced in 2008 and developed for bacteria in 2011–2012 (Martinez et al., 2012, Wilson et al., 2011)) that allows critical motility parameters such as velocities and fraction of motile particles to be extracted from recordings with low signal to noise ratios. DDM uses successive images to characterize the motility of a population by calculating the temporal fluctuations of the number density over different length scales. The key parameter is the differential image correlation function (DICF), $g(q,\tau)$, which is the modulus of the difference of two Fourier-space images over a time step τ:

$$g(q,\tau) = \left\langle |I(q,t+\tau) - I(q,t)|^2 \right\rangle_t \quad (3)$$

The DICF is related to the intermediate scattering function (ISF), $f(q,\tau)$, by.

$$g(q,\tau) = A(q)[1 - f(q,\tau)] + B(q) \quad (4)$$

where $A(q)$ depends on the optics, particle shape, and mutual arrangement, and $B(q)$ represents the camera noise. For a mixed population of motile- and non-motile cells with motile fraction α, the ISF consists of a part due to Brownian motion, represented by the diffusion coefficient D, and a part due to swimming:

$$f(q,\tau) = (1-\alpha)e^{-q^2 D\tau} + \alpha e^{-q^2 Dt} \int_0^\infty dv P(v) \frac{sin(qv\tau)}{qv\tau} \quad (5)$$

where $P(v)$ is the velocity distribution function. The term due to swimming decorrelates much more quickly than that due to Brownian motion, resulting in a two-phase f that may be fit to a multi-parameter function to extract the diffusion coefficient, mean swimming speed, and fraction swimming. The advantages of this method are rapid, tracking-free determination of these key motility parameters. The disadvantages are lack of visualization, so that spurious results are difficult to identify; some comparison with manual tracking is needed. In addition, a form for the velocity distribution function needs to be specified, so some advance knowledge of swimming characteristics is needed. The technique also requires a large data volume, approximately 1000 frames at 50 frames/s for cells swimming at typical run-and-tumble speeds (10–50 μm/s).

3. Recording apparatus and software

3.1. Cameras

Commercially available cameras require trade-offs between field of view and framerate. Until recently, obtaining full 2048 × 2048 or even 1024 × 1024 pixel images at >50 frames/s required highly specialized and costly instrumentation. Although fast cameras are becoming more readily available, obtaining frame rates >50 fps usually requires some downsampling as well as limiting any simultaneous data imaging. Cameras for fluorescence represent a special category, as they must be extremely sensitive and have low background; most are cooled. If specialized wavelengths such as ultraviolet or infrared are imaged, this imposes additional demands upon the camera. Because of the complexity of the trade-offs, we have identified the camera model in all of the studies identified in Tables 1 and 2.

The effect of framerate on analysis of bacterial tracks has been discussed in the context of a velocity jump process model, where identification of re-orientation events is key to accurate parameter estimation. As the sampling rate becomes so slow that multiple re-orientation events between frames become probable, there is a rapid breakdown in analysis accuracy (Harrison and Baker, 2018).

3.2. Acquisition software

Acquisition software is dependent on the microscopy technique chosen. For most applications, the camera software is sufficient; a software development kit (SDK) is usually provided with camera purchase. Manufacturers often sell software separately, but the cost of the software

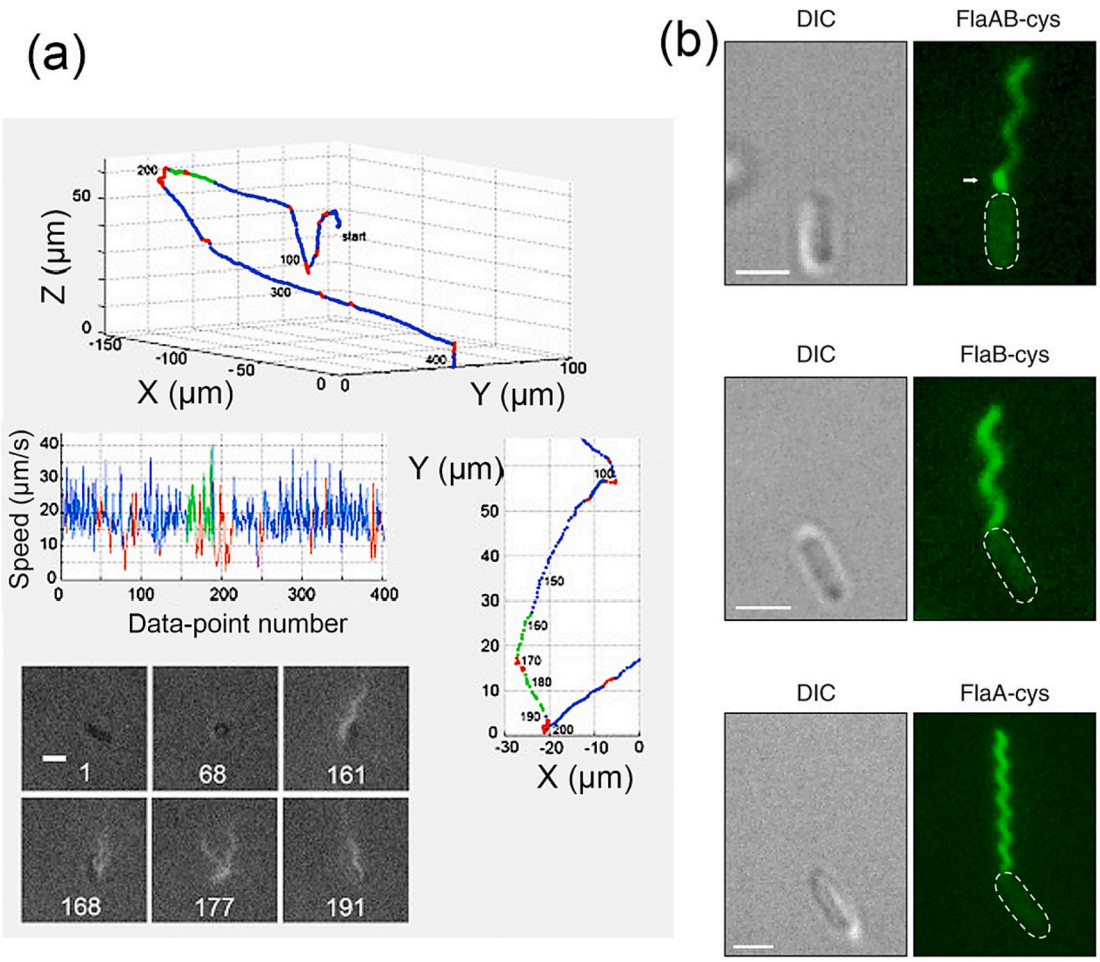

Fig. 5. Use of fluorescence microscopy and flagellar labeling to elucidate the role of flagella in swimming. (a) Track of a typical untreated *E. coli* cell (upper panel) with combined phase-contrast and fluorescence images (dark and light, respectively, lower-left panel). Runs are shown in blue, tumbles are in red, and runs with the laser on are in green. Each data point along the trajectory corresponds to one video frame (30/s). At the start, image 1 (lower-left panel), the phase-contrast image shows the cell moving parallel to the X-Y image plane. Cell-body measurements were made from this image. At image 68, the cell is seen end-on while moving along the Z axis at track point 68. The overview (right panel) shows the track in the X-Y plane from points 100–200, and includes laser illumination points 157–191. The cell was running with a tight bundle in image 161. A tumble occurred during points 168–177. In image 177, as the tumble ended, the bundle started to reform, a process that was completed at point 188 (not shown). A tightly formed bundle is evident in image 191. After this point, another tumble began. The scale bar is 2 μm (FromBiophys J. 2016 Aug 9; 111(3): 630–639. doi: https://doi.org/10.1016/j.bpj.2016.05.053, © 2016 Biophysical Society, used with permission). (b) Micrographs of cells with fluorescently labeled flagellar filaments displaying the outcome of the genetic editing of the flagellin genes (from Kuhn et al., 2018, under terms of the Creative Commons license). (For interpretation of the references to colour in this figure legend, the reader is referred to the web version of this article.)

sometimes exceeds that of the camera. The open-source package MicroManager (Edelstein et al., 2010) has been developed to interface with a large number of commercial cameras, microscopes, and accessories in order to minimize costs associated with software.

For specialized techniques such as DHM, software is usually custom. Several research groups, including our own, have made their DHM software openly available (Fregoso et al., 2020; Zhang et al., 2015).

4. Cell identification and tracking

Creating and finding tools for cell tracking is an ongoing area of development. In 2012 a "Cell Tracking Challenge" was hosted by the IEEE International Symposium on Biomedical Imaging (ISBI). The results were published in 2014 (Chenouard et al., 2014) with the statement "at present, there exists no universally best method for particle tracking," and this is still valid today, nearly a decade later.

Large datasets are generated from imaging and recording samples. One of the primary challenges for bacterial tracking relates to its low signal to noise ratios. There are a variety of both in-house and commercially available software packages that attempt to solve this problem. However, there is currently no "black box" solution that works for any bacterial dataset. Cell tracking in 2D and 3D consists of 1) preprocessing the images, 2) detecting the cells and 3) cell tracking by linking them correctly in successive video frames. Step 1 is usually semi-automated, whereas steps 2 and 3 can be done manually or automatically.

4.1. Preprocessing

The preprocessing necessary is highly dependent upon the technique used. For most brightfield and phase contrast techniques, some sort of background subtraction using different denoising approaches (rolling ball algorithm, median, Gaussian filter) is necessary. Such filters are found in all common image-processing software packages, both open-source and commercial.

For DHM, aberration correction is essential. A large amount of research has gone into development of experimental and software techniques for improvement of DHM contrast. The denoising approaches to amplitude and phase images are different. While amplitude images are generally noisier than phase images, especially with respect to

Table 2
Parameters used in some recent bacterial tracking studies using fluorescence microscopy.

Microorganism studied	Objective (s)	Fluorophore	Camera	Tracking method
E. coli[a]	100×/ NA 0.9	Yellow fluorescent protein YFP	ANDOR iXon 897 EMCCD (30 fps at 512 × 512)	Lagrangian tracker (motorized stage, photobleaching correction)
E. coli[b]	60×/NA 1.27	Red fluorescent protein mRFP1	Hamamatsu Orca Flash 4.0 (50 fps)	Custom software, confined channels
E. coli *P. aeruginosa*[c]	40×, NA 1.0	Vybrant Dyecycle Green	Zeiss, 80 ms exposure	Segmentation and LAP tracking
E. coli *B. subtilis* *Enterococcus*[d]	25× LWD/ NA 1.1	Alexa Fluor 532 maleimide (flagellar labeling)	KPC-650BH (30 fps)	Tracking microscope

[a] Figueroa-Morales et al. Physical Review X 2020, 10, (2), 021004.
[b] Vizsnyiczai et al. Nat Commun 2020, 11, (1), 2340.
[c] Khong et al. bioRxiv 2020, 2020.05.03.075507.
[d] Turner et al. Biophysical Journal 2016, 111, (3), 630–639.

speckle noise, approaches to de-noising are simpler. If the fringes are temporally stable, the hologram may be median subtracted before reconstruction in amplitude (Bedrossian et al., 2020) (Fig. 6 (a)-(c)). Alternatively, amplitude images may be median subtracted plane-by-plane after reconstruction. For motile objects, this usually results in sufficient de-noising for particle detection. Additional signal-to-noise may be obtained using frame-to-frame subtraction, a method which is frequently used for DIHM. These techniques remove motionless objects, which can be an advantage or a disadvantage depending upon the experiment.

Quantitative phase retrieval presents specific challenges; approaches to phase aberration correction have been recently reviewed (Sirico et al., 2022). Digital aberration correction is usually performed using a reference hologram (Colomb et al., 2006), but this reference must be chosen carefully. If objects are moving, a good reference hologram may be the median of the entire image stack, provided that the fringes are stable (Fig. 6 (d)). For long acquisitions or when fringes are not stable, a "rolling mean" of a selected number of images may serve as a reference hologram. Obtaining an empty reference from a chamber without cells is usually not possible, since many of the aberrations arise from the precise sample chamber and area of the chamber being imaged. Thus, even microscopic changes in the slide position can alter the aberrations.

An advantage of phase reconstructions is the Gouy phase anomaly, where an object switches from light to dark across the focal plane (Fig. 6 (e)). This means that the Z-derivative has a maximum at that point, so the axial derivative of a phase reconstruction reduces noise in Z (Fig. 6 (f)) and in XY (Fig. 6 (g)). The choice of reconstruction spacing for the derivative depends upon the dataset (Gibson et al., 2021).

For 3D datasets of all types, *deconvolution* may be necessary to improve axial resolution, which is lower than lateral resolution for all microscopic techniques. Deconvolution is based upon knowing the shape of the point-spread function (PSF) for the microscope system, and reducing each PSF in the image to a point based upon this input. Exact algorithms depend upon the particular parameters of the PSF and the noise, and so are specific to each microscopy technique. Comprehensive, practical reviews are available for brightfield microscopy and fluorescence microscopy (Goodwin, 2014; Swedlow, 2013), as well as for more specialized techniques such as light sheet microscopy (Becker et al., 2019). The PSF may be experimentally measured by imaging unresolved point particles, or may be theoretically calculated based upon the optics of the microscope. Theoretical modeling of the PSF is done within the software with the user supplying values such as the objective lens,

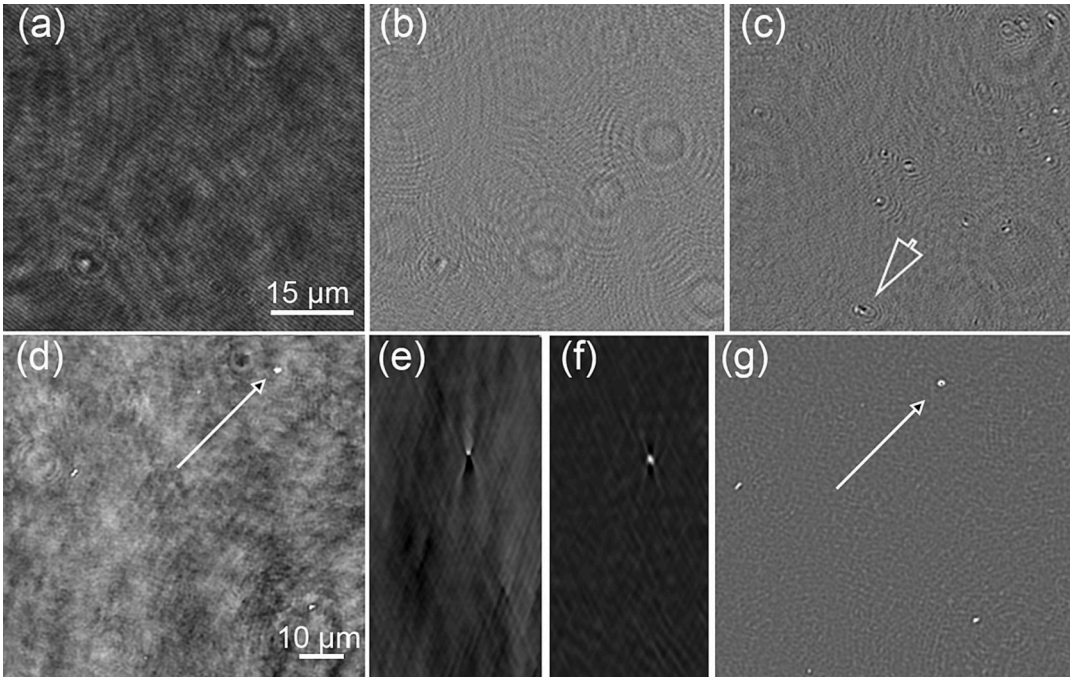

Fig. 6. Appearance of bacteria (in this case, the marine microorganism *Collwellia psychrerythraea* 34H) under DHM with and without denoising. (a) Raw hologram of part of the microscopic field of view. (b) Median subtracted hologram (as in (Bedrossian et al., 2020)) showing individual cells whose Airy patterns overlap in Z. (c) Reconstruction on a single focal plane in amplitude. Cells in focus (arrow) are reduced to 1–2 pixels, while cells not in focus in that plane retain large diffraction patterns. (d) Phase reconstruction on a single Z plane, with an example cell indicated by an arrow, using a reference hologram that is the mean of the entire stack. (e) YZ image through a stack of phase images reconstructed every 1 μm, showing the Gouy phase anomaly. (f) Derivative image of cell in the YZ plane. (g) Derivative image of the same plane in XY with arrow indicating the same cell as in Panel (d).

immersion medium, and illumination wavelength. Commercial packages and open-source plug-ins are available for deconvolution of fluorescence and brightfield images (Table 3).

4.2. Cell detection

Cell detection consists of recognizing pixel clusters of a defined size, which stand out from the background in a way that may be identified by an algorithm. Frequently, but not always, images are thresholded and converted to binary before tracking. Thresholding of fluorescence images is fairly straightforward, but for low signal-to-noise techniques such as brightfield and DHM, cell detection may be the most challenging aspect of the data analysis. A recent review provided a detailed overview of techniques and software for microbial image analysis, including both single cell and community analysis (Jeckel and Drescher, 2021). For most tracking purposes, cells must be accurately identified frame by frame; thus, the detection step is independent of, but necessary to, the tracking step.

4.2.1. Detection by thresholding

Because of the presence of Airy rings, phase contrast and DHM images cannot be thresholded readily (Fig. 7 (a)-(c)). The edges of the Airy rings are detected more easily by particle detection algorithms than the in-focus cells. Reconstructions of median-subtracted holograms, phase derivatives, or projections across multiple Z planes all permit thresholding for some datasets (with no general rule applicable to all). Projections across Z planes may be sums of all slices, maximum projections, or minimum projections, again depending upon the dataset. Thresholding based upon maximum entropy yields the best results for most brightfield images (Fig. 7 **(d)-(f)**).

4.2.2. Other methods

Features other than simple grayscale contrast may be used to distinguish cells from background. Some features that can be used are edge, texture, gradient, and structure. Depending on the algorithm, several features may be combined.

Despite the availability of these tools, optimizing parameters can be time-consuming or even futile. Differences in noise or cell density from frame to frame, and changes in bacterial appearance with tumbling or other motions, can lead to poor classification. Machine learning approaches can help to optimize the many parameters needed for effective tracking; the machine learning package in MATLAB has been used to detect *Bacillus subtilis* (Manuel et al., 2018). The training can be extensive and highly dataset-dependent (Deter et al., 2019; O'Connor et al., 2022) (Meacock and Durham, 2022), and a recent paper proposed an adaptive kernel model for addressing these challenges and applied it to *E. coli* (Xie et al., 2008). For all of these methods, generalizability is challenging; what works for *E. coli* often does not work with smaller, faster microorganisms, such as *Vibrio*.

Convolutional neural networks (CNNs) are a type of machine learning algorithm that learns directly from image data. MATLAB includes a Deep Learning Toolbox that can be used to design, train, and apply CNNs. New software packages have also recently been reported for submicron particle tracking which have been shown to recognize non-spherical cells such as *Salmonella* (Newby et al., 2018).

4.3. Cell tracking

After particle identification, tracking still poses a challenge. While excellent tools exist for analyzing passive motion, such as Brownian motion, simple techniques such as nearest neighbor linking over the smallest Euclidean distance cannot be used for particle tracking with partly fast-moving, strongly accelerating microbes. Particle tracks intersect and overlap, and velocity vectors are unpredictable. Therefore, the linking step is often done using a cost (or energy) function that takes into account velocity aspects (such as smoothness of the trajectory

Table 3
Selected software packages for image processing, bacterial detection, and tracking.

Software	Task	Platform	Availability
TrackMate[a]	Particle identification and tracking	Fiji	Open source
Arivis Vision 4D[b]	Many filters and tracking algorithms; handles large 4D stacks	Win	Commercial
MOSAICSuite[c]	Particle detection and tracking	Fiji	Open source
Ilastik[d]	Machine learning for segmentation	Fiji	Open source
MorphoLibJ[e]	Morphology analysis	Fiji	Open source
SuperSegger[f]	Cell segmentation (fluorescence)	MATLAB	Free
MicrobeJ[g]	Cell detection and analysis; large datasets	Fiji	Open source
DeepBacs[h]	Deep learning segmentation for fluorescence & brightfield	Jupyter	
Zcells[i]	Machine-learning based segmentation	MATLAB	Free
TumbleScore[j]	Bacterial tracking and track analysis	MATLAB	Free
Your Software for Motility Recognition[k]	High-throughput bacterial identification and tracking	Python	Open source
Bacterial swarming[l]	Swarming segmentation and analysis	MATLAB	Free
AI Tracking solutions[m]	CNN-based tracking	Cloud-based	Commercial
Machine Learning Object Tracking (MLOT)[n]	Machine learning based identification	MATLAB	Free
TaxisPy[o]	Chemotaxis analysis	Python	Free
DHM[p]	DHM reconstruction/ simulation	Fiji	Open source
DHM Utilities[q]	DHM reconstruction with reference hologram options	Fiji	Open source
KOALA[r]	DHM reconstruction with reference hologram options	Win	Commercial
Iterative Deconvolve 3D[s]	Deconvolution	Fiji	Open source
DeconvolutionLab2[t]	Deconvolution	Fiji	Open source
Huygens[u]	Deconvolution	Cross-platform (Win, Mac, Linux)	Commercial

[a] D. Ershov *et al.*, Nat Methods **19**, 829 (2022).
[b] https://www.arivis.com/solutions/vision4d
[c] I. F. Sbalzarini and P. Koumoutsakos, Journal of Structural Biology **151**, 182 (2005).
[d] S. Berg *et al.*, Nat Methods **16**, 1226 (2019).
[e] D. Legland et al., Bioinformatics **32**, 3532 (2016).
[f] S. Stylianidou et al., Mol Microbiol **102**, 690 (2016).
[g] A. Ducret et al., Nat Microbiol **1**, 16,077 (2016).
[h] C. Spahn *et al.*, Commun Biol **5**, 688 (2022).
[i] https://lab513.github.io/Zcells/
[j] A. E. Pottash et al., Biotechniques **62**, 31 (2017).
[k] J. Schwanbeck et al., BMC Bioinformatics **21**, 166 (2020).
[l] A. Be'er et al., Communications Physics **3**, 66 (2020).
[m] https://aitracker.net/
[n] https://github.com/mbedross/MachineLearningObjectTracking
[o] M. A. Valderrama-Gomez et al., J Microbiol Methods **175**, 105,918 (2020).
[p] https://github.com/unal-optodigital/DHM/blob/master/README.md
[q] https://github.com/sudgy
[r] https://www.lynceetec.com/koala-acquisition-analysis/
[s] https://imagej.net/plugins/iterative-deconvolve-3d
[t] Sage *et al. Methods* **115**, 28–41, doi:https://doi.org/10.1016/j.ymeth.2016.12.015 (2017).

[u] https://svi.nl/Huygens-Software

segment, smoothness of 3D velocity, smoothness, and upper bound conditions on accelerations) or morphological characteristics (cell size, shape, aspect). That means it requires *a priori* information about the microbes. However, the correct weighting of all the different features of the cost function is often highly dependent on the used set-up and requires a lot of fine-tuning.

4.3.1. Manual tracking

Manual tracking was the only possible approach before the development of high-performance computers (Berg and Brown, 1972; Schneider and Doetsch, 1974). Even with modern computation, it is still in widespread use, either as a stand-alone technique or to "ground truth" automated methods. Computational tools can assist with manual tracking by annotating and saving tracks. The technique is tedious and is frequently outsourced to data analysts or assigned to undergraduate students. Throughput is low.

4.3.2. Automated tracking

Automated tracking greatly decreases the workload and improves statistics. Common algorithms are discussed below.

The Linear Assignment Problem (LAP) tracker, published in 2008, helps solve the problems of trajectory overlap, particle disappearance from frame to frame, and trajectory merging and splitting(Jaqaman et al., 2008). Identified particles are linked frame to frame, then segments are linked to create trajectories. In order to determine whether segments belong to the same trajectory, a "cost matrix" is used representing all of the possibilities for spots in one frame to be linked to spots in the next. The matrix is minimized to create the most probable set of trajectories. In most software implementations, the user can fine-tune the algorithm by specifying the maximum number of frames across which to link, and the maximum number of pixels traveled by a microorganism between frames. These parameters are obviously highly dependent upon the speed of the microorganism relative to the camera frame rate. For a heterogeneous mix of microorganisms of different speeds, the tracker may need to be re-run with different parameters to optimize linking for each cell type. The ability of the detection algorithm to find the cell in each frame will also influence the gap-closing parameter.

A second approach relies on a Kalman filter, reported in the same paper as the LAP tracker (Jaqaman et al., 2008), to predict the most probable position of a particle assuming that it moves with a constant velocity. The same cost matrix is used as for LAP tracking, using the square distance as cost; the software should allow manual input of test values for this initial distance. The predicted positions are linked against the actual positions of particles in each successive frame.

Even for a homogeneous culture of a single bacterial species, there are some trajectories that are better captured with a LAP tracker (e.g., those with turns or spirals), and those better captured with the Kalman tracker (long runs) (Fig. 8). In all cases, several iterations will likely be necessary to optimize gap-closing distances, and manual editing and stitching/cutting of tracks can further improve results after the automated detection.

Software packages of particular relevance to all steps of data processing, bacterial identification and tracking are tabulated in Table 3.

4.4. Considerations for 3D

3D tracking of microbial motility can lead to more accurate velocity measurements as well as reveal features that are obscured by 2D projections, especially dynamic surface behavior (Bianchi et al., 2019) (Taute et al., 2015). However, 3D tracking poses particular difficulties, and so full 3D tracked datasets of micron-sized organisms are sparse. The two biggest issues with 3D tracking are (1) poorer axial resolution vs XY

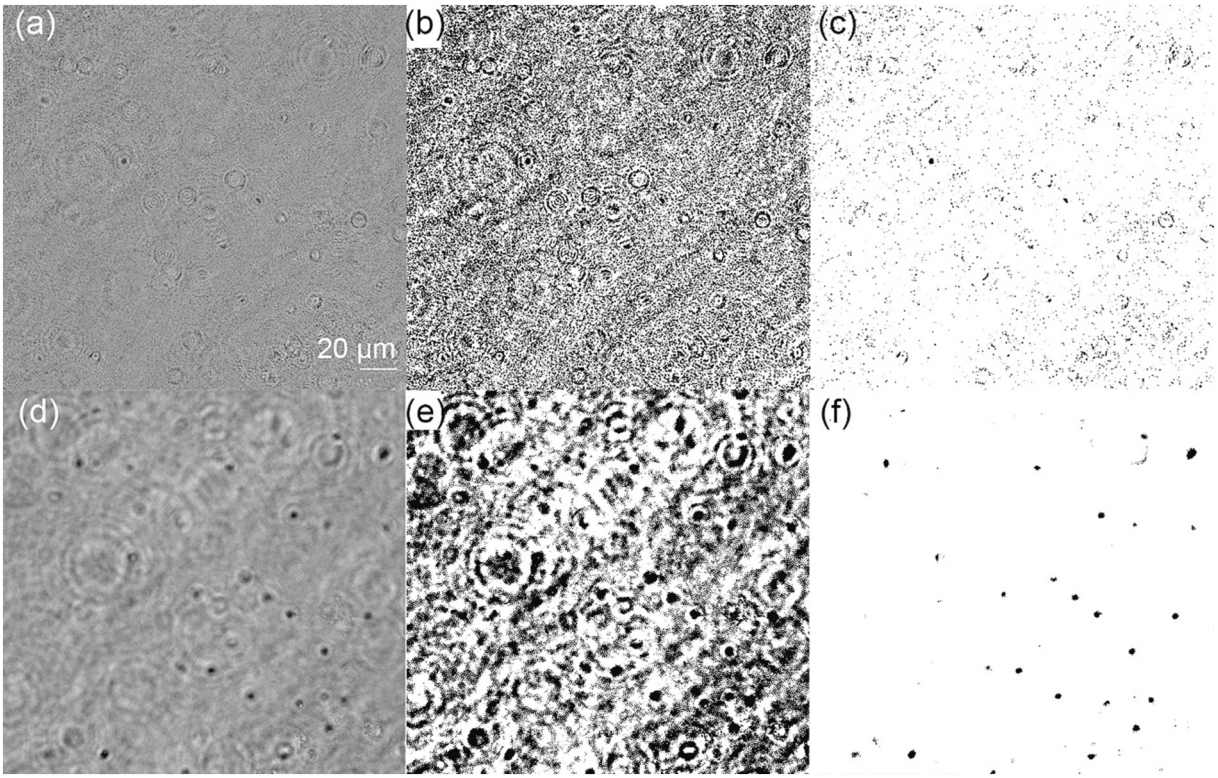

Fig. 7. Thresholding DHM images of the bacterium *Shewanella putrefaciens*. (a) Amplitude reconstruction on a single focal plane. (b) Thresholding using the "default" algorithm in Fiji. (c) Thresholding using the "Max Entropy" algorithm in Fiji. (d) Sum of multiple Z planes from the same field of view. (e) Thresholding using the "default" algorithm. (f) Thresholding using Max Entropy identifies the majority of the cells and can be used for tracking.

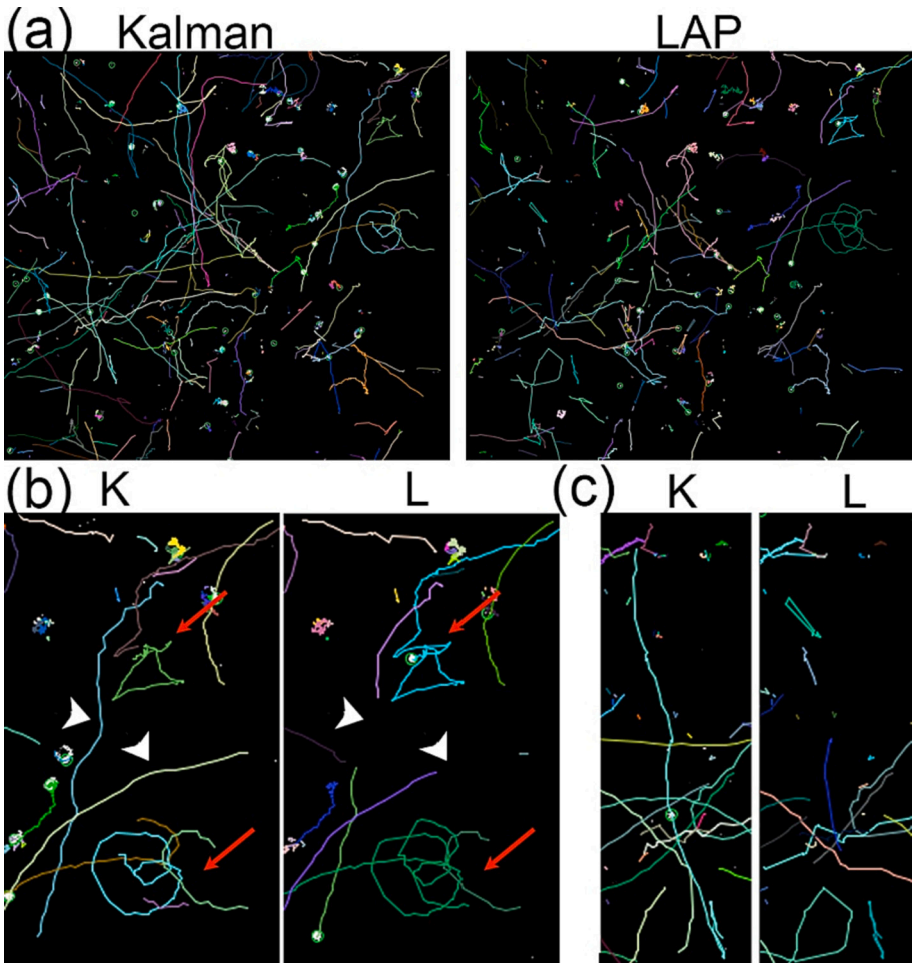

Fig. 8. Kalman vs. LAP tracker for DHM data using the microorganism *Shewanella putrefaciens*. (a) Large field of view indicating how it is possible to tell at a glance that the Kalman filter detects more long runs than the LAP tracker. (b) 2-fold zoom of upper right of image, showing circuitous tracks that were captured as single tracks by the LAP tracker but not the Kalman filter (red arrows), vs. long runs that were successfully captured by the Kalman filter but broken in the LAP tracker (white arrowheads). (c) 2-fold zoom of lower left corner showing a long track apparent in the Kalman filter (turquoise) that was entirely missed by the LAP tracker. The accuracy of the assignments must be checked by eye (see Supplementary Videos 1 and 2 for animations of Panel (a)). (For interpretation of the references to colour in this figure legend, the reader is referred to the web version of this article.)

resolution with most microscopic techniques; and (2) large dataset size. The use of supercomputers and software/file types specifically designed for handling large datasets can permit tracking of full resolution (2048x2048x100 XYZ) data, but usually either downsampling, cropping, or truncation of time series is necessary. Truncation or cropping may be designed to isolate a specific cell. Stitching may be done in spatial or time coordinates depending upon which is easier for the given data.

Alternatives to tracking of full 3D datasets include:

- 2D tracking of Z-projections followed by manual extraction of Z coordinates (Fig. 9 (a), Supplementary Video 3) (Acres and Nadeau, 2021).
- 2D tracking of Z-projections followed by automated extraction of Z coordinates by fitting or measuring Airy rings; may be done for phase contrast and DHM (Fig. 9 (b), Supplementary Video 4). For DHM, a simulated PSF may be created by angular spectrum propagation of a single-pixel spot (Piedrahita-Quintero et al., 2015) (Fig. 9 (c), (d)), and then used to match experimental data (Fig. 9 (e)).
- Tracking of XY and XZ or YZ projections, then matching corresponding coordinates to obtain full XYZ information. However, the overlapping coordinates to obtain full tracks can be challenging; this approach is much more efficient with passive motion, where corresponding X or Y coordinates can be readily mapped (Rouzie et al., 2021).

Note that none of these approaches are high throughput. All require substantial cropping of the datasets to make them manageable in size, as well as user input to ensure that the correct cell is tracked throughout the length of its appearance in the volume of view.

4.5. Analyzing tracks

Unlike simple physical motion such as Brownian motion, active motility displays both physical and physiological features that have not been fully elucidated. To mention a few examples, the run-reverse-flick swimming pattern of bacteria with a single polar flagellum was not described until 2011 (Stocker, 2011b). Persistence in tracks was first reported in 2013 (Rosser et al., 2013). Tumbling frequencies near a surface, suggesting chemotactic behavior, were reported in 2020 (Lemelle et al., 2020). The biophysics underlying bacterial motility can be lost if tracks are fragmented, spurious, or if they miss key features such as reorientation events. There is no established standard for quantifying bacterial reorientations. Because of the different possible motility patterns as shown in Fig. 1, such analysis must be strain-dependent. This becomes increasingly challenging if the culture represents a mix of species. All tracking methods lead to some degree of false negative and false positive detection, and all require manual editing to stitch fragmented tracks or separate spuriously joined tracks. In some cases, this will require almost as much work as full manual tracking.

Parameters that may need to be quantified include run lengths, tumbles and/or reversals, turn angles, velocity, acceleration, and correlation coefficients. All of these parameters, if they are reported as averages over individual tracks, can be highly misleading if the tracks are spuriously truncated, joined, or split. Another aspect that must be considered is that bacterial cultures contain some fraction of non-motile cells, and the extent to which these should be analyzed or excluded from analysis depends upon the experiments and the hypotheses being tested.

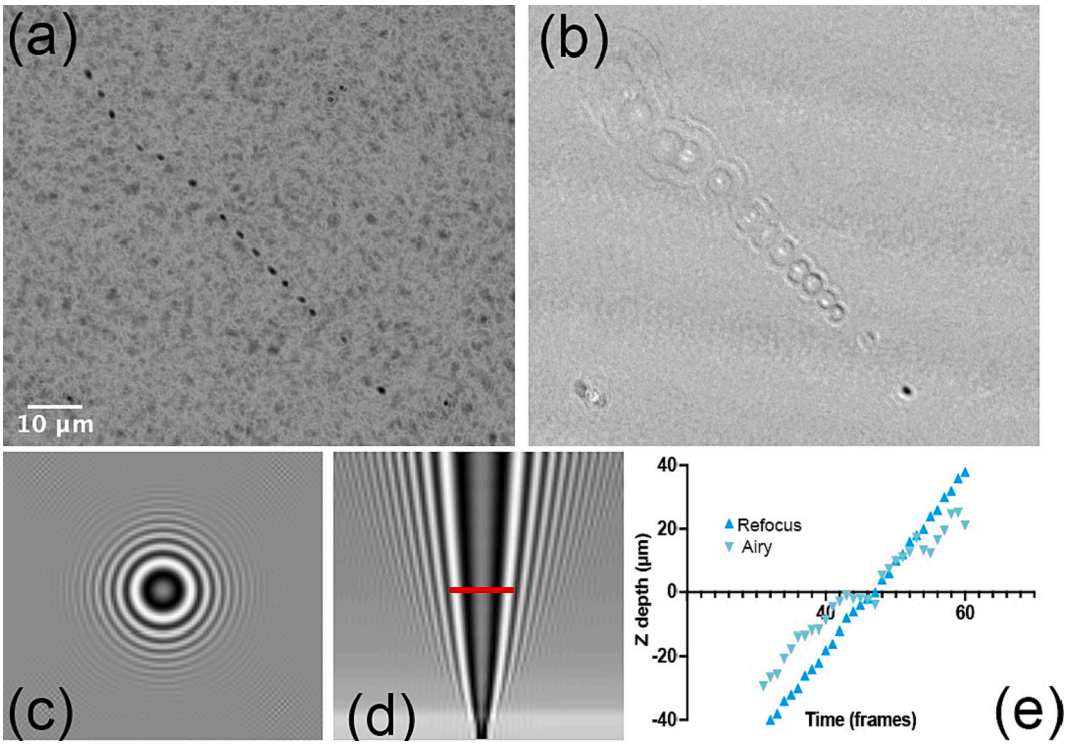

Fig. 9. Obtaining Z coordinates from DHM reconstructions. (a) Minimum intensity projection of 30 frames of a single cell, choosing the z plane at which the cell is in best focus (all slices shown in Supplementary Video 3). (b) Minimum plus maximum intensity projection for the same cell from a reconstruction at a single focal plane (all slices shown in Supplementary Video 4). (c) Simulated Airy rings in the XY plane for a point source projected over 30 μm in Z, using angular spectrum propagation with the same optical parameters as the instrument used to collect the experimental data. (d) Simulated Airy rings in the YZ plane; the red line indicates the area that was used to estimate depth for the cell at each time point. (e) Depth obtained with time for the tracked cell, comparing the refocusing and Airy ring approaches. (For interpretation of the references to colour in this figure legend, the reader is referred to the web version of this article.)

The degree to which false negatives/positives and broken tracks can be tolerated also depends upon what is being studied.

When tracks are correctly identified and exported as XYT or XYZT coordinates, parameters such as velocities and accelerations may be readily calculated from their definitions. However, evaluation of complex behaviors such as chemotaxis (Pohl et al., 2017) and tumbling (Liang et al., 2018) require models and model-based parameters, and their analysis can be assisted by specialized software packages as indicated in Table 3.

5. Conclusion

Tracking bacteria still represents a challenge, especially in 3D or under extreme conditions such as high or low temperature, high cell speed, or dense or inhomogeneous cultures (mixed species or phenotypes). Each experimental type, or even each dataset, will require customized methods and ground-truthing to eliminate false negatives and false positives. Manual tracking remains a necessary task for many applications, since the human eye and brain can identify cells and motion in noisy environments where even the most sophisticated algorithms fail. Modeling the physics of motility can be influenced by false positives, false negatives, and broken tracks. Improvements in 3D tracking will lead to new discoveries in the physics of microbial motility.

Supplementary data to this article can be found online at https://doi.org/10.1016/j.mimet.2022.106658.

Declaration of Competing Interest

The authors declare that they have no known competing financial interests or personal relationships that could have appeared to influence the work reported in this paper.

Data availability

Data will be made available on request.

Acknowledgements

The authors acknowledge the support of the National Science Foundation (Grant No. 1828793). Portions of this work were supported under a contract from the Jet Propulsion Laboratory, California Institute of Technology, under a contract with the National Aeronautics and Space Administration.

References

Acres, J., Nadeau, J., 2021. 2D vs 3D tracking in bacterial motility analysis. AIMS Biophys. 8, 385–399.
Albers, S.V., Jarrell, K.F., 2015. The archaellum: how Archaea swim. Front. Microbiol. 6, 23.
Albers, C.N., Kramshøj, M., Rinnan, R., 2018. Rapid mineralization of biogenic volatile organic compounds in temperate and Arctic soils. Biogeosciences. 15, 3591–3601.
Armitage, J.P., 1999. Bacterial tactic responses. In: Poole, R.K. (Ed.), Advances in Microbial Physiology, vol. 41. Academic Press, pp. 229–289.
Armitage, J.P., Schmitt, R., 1997. Bacterial chemotaxis: rhodobacter sphaeroide and *Sinorhizobium meliloti* - variations on a theme? Microbiology. 143, 3671–3682.
Bardy, S.L., Briegel, A., Rainville, S., Krell, T., 2017. Recent advances and future prospects in bacterial and archaeal locomotion and signal transduction. J. Bacteriol. 199. JB.00203-00217.
Becker, K., Saghafi, S., Pende, M., Sabdyusheva-Litschauer, I., Hahn, C.M., Foroughipour, M., Jahrling, N., Dodt, H.U., 2019. Deconvolution of light sheet microscopy recordings. Sci. Rep. 9, 17625.
Bedrossian, M., Wallace, J.K., Serabyn, E., Lindensmith, C., Nadeau, J., 2020. Enhancing final image contrast in off-axis digital holography using residual fringes. Opt. Express 28, 16764–16771.
Bente, K., Mohammadinejad, S., Charsooghi, M.A., Bachmann, F., Codutti, A., Lefevre, C. T., Klumpp, S., Faivre, D., 2020. High-speed motility originates from cooperatively pushing and pulling flagella bundles in bilophotrichous bacteria. Elife. 9.
Berg, H.C., 1971. How to track bacteria. Rev. Sci. Instrum. 42, 868–871.

Berg, H.C., Brown, D.A., 1972. Chemotaxis in *Escherichia coli* analysed by three-dimensional tracking. Nature. 239, 500–504.
Berg, H.C., Brown, D.A., 1974. Chemotaxis in *Escherichia coli* analyzed by three-dimensional tracking. Antibiot. Chemother. (1971) 19, 55–78.
Bernas, T., Zarebski, M., Dobrucki, J.W., Cook, P.R., 2004. Minimizing photobleaching during confocal microscopy of fluorescent probes bound to chromatin: role of anoxia and photon flux. J. Microsc. 215, 281–296.
Bianchi, S., Saglimbeni, F., Frangipane, G., Dell'Arciprete, D., Di Leonardo, R., 2019. 3D dynamics of bacteria wall entrapment at a water-air interface. Soft Matter 15, 3397–3406.
Boquet-Pujadas, A., Olivo-Marin, J.C., Guillen, N., 2021. Bioimage Analysis and Cell Motility. Patterns (N Y). 2, 100170.
Boudreau, C., Wee, T.L., Duh, Y.R., Couto, M.P., Ardakani, K.H., Brown, C.M., 2016. Excitation light dose engineering to reduce photo-bleaching and photo-toxicity. Sci. Rep. 6, 30892.
Buitrago-Duque, C., Garcia-Sucerquia, J., 2022. Realistic simulation and real-time reconstruction of digital holographic microscopy experiments in ImageJ. Appl. Opt. 61, B56–B63.
Charles-Orszag, A., Lord, S.J., Mullins, R.D., 2021. High-temperature live-cell imaging of cytokinesis, cell motility, and cell-cell interactions in the thermoacidophilic crenarchaeon *Sulfolobus acidocaldarius*. Front. Microbiol. 12, 707124.
Chenouard, N., Smal, I., de Chaumont, F., Maska, M., Sbalzarini, I.F., Gong, Y., Cardinale, J., Carthel, C., Coraluppi, S., Winter, M., Cohen, A.R., Godinez, W.J., Rohr, K., Kalaidzidis, Y., Liang, L., Duncan, J., Shen, H., Xu, Y., Magnusson, K.E., Jalden, J., Blau, H.M., Paul-Gilloteaux, P., Roudot, P., Kervrann, C., Waharte, F., Tinevez, J.Y., Shorte, S.L., Willemse, J., Celler, K., van Wezel, G.P., Dan, H.W., Tsai, Y.S., Ortiz de Solorzano, C., Olivo-Marin, J.C., Meijering, E., 2014. Objective comparison of particle tracking methods. Nat. Methods 11, 281–289.
Cheong, F.C., Sun, B., Dreyfus, R., Amato-Grill, J., Xiao, K., Dixon, L., Grier, D.G., 2009. Flow visualization and flow cytometry with holographic video microscopy. Opt. Express 17, 13071–13079.
Chia, H.E., Marsh, E.N.G., Biteen, J.S., 2019. Extending fluorescence microscopy into anaerobic environments. Curr. Opin. Chem. Biol. 51, 98–104.
Chia, H.E., Zuo, T., Koropatkin, N.M., Marsh, E.N.G., Biteen, J.S., 2020. Imaging living obligate anaerobic bacteria with bilin-binding fluorescent proteins. Curr. Res. Microb. Sci. 1, 1–6.
Cohoe, D., Hanczarek, I., Wallace, J.K., Nadeau, J., 2019. Multiwavelength digital holographic imaging and phase unwrapping of protozoa using custom Fiji Plug-ins. Front. Phys. 7.
Colomb, T., Kuhn, J., Charriere, F., Depeursinge, C., Marquet, P., Aspert, N., 2006. Total aberrations compensation in digital holographic microscopy with a reference conjugated hologram. Opt. Express 14, 4300–4306.
Corkidi, G., Taboada, B., Wood, C.D., Guerrero, A., Darszon, A., 2008. Tracking sperm in three-dimensions. Biochem. Biophys. Res. Commun. 373, 125–129.
Davidson, M.W., Spring, K.R.. Nikon Microscopy U. https://www.microscopyu.com/microscopy-basics/depth-of-field-and-depth-of-focus.
de Chaumont, F., Dallongeville, S., Chenouard, N., Herve, N., Pop, S., Provoost, T., Meas-Yedid, V., Pankajakshan, P., Lecomte, T., Le Montagner, Y., Lagache, T., Dufour, A., Olivo-Marin, J.C., 2012. Icy: an open bioimage informatics platform for extended reproducible research. Nat. Methods 9, 690–696.
Deter, H.S., Dies, M., Cameron, C.C., Butzin, N.C., Buceta, J., 2019. A cell segmentation/tracking tool based on machine learning. Methods Mol. Biol. 2040, 399–422.
Dubay, M.M., Johnston, N., Wronkiewicz, M., Lee, J., Lindensmith, C.A., Nadeau, J.L., 2022. Quantification of Motility in Bacillus subtilis at Temperatures Up to 84°C Using a Submersible Volumetric Microscope and Automated Tracking Frontiers in Microbiology, p. 13.
Edelstein, A., Amodaj, N., Hoover, K., Vale, R., Stuurman, N., 2010. Computer control of microscopes using microManager. Curr. Protoc. Mol. Biol. Chapter 14 (Unit14), 20.
El Najjar, N., van Teeseling, M.C.F., Mayer, B., Hermann, S., Thanbichler, M., Graumann, P.L., 2020. Bacterial cell growth is arrested by violet and blue, but not yellow light excitation during fluorescence microscopy. BMC Mol. Cell Biol. 21, 35.
Emami, N., Sedaei, Z., Ferdousi, R., 2021. Computerized cell tracking: current methods, tools and challenges. Vis. Inform. 5, 1–13.
Farhadi, A., Bedrossian, M., Lee, J., Ho, G.H., Shapiro, M.G., Nadeau, J.L., 2020. Genetically encoded phase contrast agents for digital holographic microscopy. Nano Lett. 20, 8127–8134.
Fregoso, S.F., Lima, F., Wallace, J.K., Bedrossian, M., McKeithen, D., Kettenbeil, C., Loya, F., Lindensmith, C., 2020. DHMx (Digital Holographic Microscope Experience) Software Tool, Imaging and Applied Optics Congress. Optica Publishing Group, Washington, DC. HF2G.7.
Frymier, P.D., Ford, R.M., Berg, H.C., Cummings, P.T., 1995. Three-dimensional tracking of motile bacteria near a solid planar surface. Proc. Natl. Acad. Sci. U. S. A. 92, 6195–6199.
Gahlmann, A., Moerner, W.E., 2014. Exploring bacterial cell biology with single-molecule tracking and super-resolution imaging. Nat. Rev. Microbiol. 12, 9–22.
Galande, A.S., Thapa, V., Ram, H.P., John, R., 2021. Untrained neural network with explicit denoiser for lensless inline holographic microscopy. In: H. J. B. M.-C. M. M. O. S. A. T. S. A. T. K. J. W. F. O. F. S. P. B. P, Hua, O. Korotkova (Eds.), OSA Imaging and Applied Optics Congress 2021 (3D, COSI, DH, ISA, pcAOP). Optica Publishing Group, Washington, DC. CTh7A.7.
Gibson, T., Bedrossian, M., Serabyn, E., Lindensmith, C., Nadeau, J.L., 2021. Using the Gouy phase anomaly to localize and track bacteria in digital holographic microscopy 4D images. J. Opt. Soc. Am. A Opt. Image Sci. Vis. 38, A11–A18.
Giloh, H., Sedat, J.W., 1982. Fluorescence microscopy: reduced photobleaching of rhodamine and fluorescein protein conjugates by n-propyl gallate. Science. 217, 1252–1255.
Goodwin, P.C., 2014. Quantitative deconvolution microscopy. Methods Cell Biol. 123, 177–192.
Harrison, J.U., Baker, R.E., 2018. The impact of temporal sampling resolution on parameter inference for biological transport models. PLoS Comput. Biol. 14, e1006235.
Herzog, B., Wirth, R., 2012a. Swimming behavior of selected species of Archaea. Appl. Environ. Microbiol. 78, 1670–1674.
Herzog, B., Wirth, R., 2012b. Swimming behavior of selected species of Archaea. Appl. Environ. Microbiol. 78, 1670–1674.
Holscher, H.D., 2017. Dietary fiber and prebiotics and the gastrointestinal microbiota. Gut Microbes 8, 172–184.
Jaqaman, K., Loerke, D., Mettlen, M., Kuwata, H., Grinstein, S., Schmid, S.L., Danuser, G., 2008. Robust single-particle tracking in live-cell time-lapse sequences. Nat. Methods 5, 695–702.
Jeckel, H., Drescher, K., 2021. Advances and opportunities in image analysis of bacterial cells and communities. FEMS Microbiol. Rev. 45.
Junge, K., Eicken, H., Deming, J.W., 2003. Motility of *Colwellia psychrerythraea* strain 34H at subzero temperatures. Appl. Environ. Microbiol. 69, 4282–4284.
Ko, S., Jeon, H., Yoon, S., Kyung, M., Yun, H., Na, J.H., Jung, S.T., 2020. Discovery of novel *Pseudomonas putida* flavin-binding fluorescent protein variants with significantly improved quantum yield. J. Agric. Food Chem. 68, 5873–5879.
Kühn, J., Niraula, B., Liewer, K., Kent Wallace, J., Serabyn, E., Graff, E., Lindensmith, C., Nadeau, J.L., 2014. A Mach-Zender digital holographic microscope with sub-micrometer resolution for imaging and tracking of marine micro-organisms. Rev. Sci. Instrum. 85, 123113.
Kuhn, M.J., Schmidt, F.K., Farthing, N.E., Rossmann, F.M., Helm, B., Wilson, L.G., Eckhardt, B., Thormann, K.M., 2018. Spatial arrangement of several flagellins within bacterial flagella improves motility in different environments. Nat. Commun. 9, 5369.
Latychevskaia, T., Fink, H.-W., 2009. Simultaneous reconstruction of phase and amplitude contrast from a single holographic record. Opt. Express 17, 10697–10705.
Lee, S.-H., Roichman, Y., Yi, G.-R., Kim, S.-H., Yang, S.-M., Blaaderen, A.V., Oostrum, P. V., Grier, D.G., 2007a. Characterizing and tracking single colloidal particles with video holographic microscopy. Opt. Express 15, 18275–18282.
Lee, S.H., Roichman, Y., Yi, G.R., Kim, S.H., Yang, S.M., van Blaaderen, A., van Oostrum, P., Grier, D.G., 2007b. Characterizing and tracking single colloidal particles with video holographic microscopy. Opt. Express 15, 18275–18282.
Lei, H., Hu, X., Zhu, P., Chang, X., Zeng, Y., Hu, C., Li, H., Hu, X., 2015. Nano-level position resolution for particle tracking in digital in-line holographic microscopy. J. Microsc. 260, 100–106.
Lemelle, L., Cajgfinger, T., Nguyen, C.C., Dominjon, A., Place, C., Chatre, E., Barbier, R., Palierne, J.F., Vaillant, C., 2020. Tumble kinematics of *Escherichia coli* near a solid surface. Biophys. J. 118, 2400–2410.
Leuko, S., Legat, A., Fendrihan, S., Stan-Lotter, H., 2004. Evaluation of the LIVE/DEAD BacLight kit for detection of extremophilic archaea and visualization of microorganisms in environmental hypersaline samples. Appl. Environ. Microbiol. 70, 6884–6886.
Liang, X., Lu, N., Chang, L.C., Nguyen, T.H., Massoudieh, A., 2018. Evaluation of bacterial run and tumble motility parameters through trajectory analysis. J. Contam. Hydrol. 211, 26–38.
Lindensmith, C.A., Rider, S., Bedrossian, M., Wallace, J.K., Serabyn, E., Showalter, G.M., Deming, J.W., Nadeau, J.L., 2016. A submersible, off-axis holographic microscope for detection of microbial motility and morphology in aqueous and icy environments. PLoS One 11, e0147700.
Liu, B., Gulino, M., Morse, M., Tang, J.X., Powers, T.R., Breuer, K.S., 2014. Helical motion of the cell body enhances *Caulobacter crescentus* motility. Proc. Natl. Acad. Sci. U. S. A. 111, 11252–11256.
Manuel, B., Marwan, E.-K., Daniel, N., Jay, N., 2018. A machine learning algorithm for identifying and tracking bacteria in three dimensions using Digital Holographic Microscopy. AIMS Biophys. 5, 36–49.
Marquet, P., Rappaz, B., Magistretti, P.J., Cuche, E., Emery, Y., Colomb, T., Depeursinge, C., 2005. Digital holographic microscopy: a noninvasive contrast imaging technique allowing quantitative visualization of living cells with subwavelength axial accuracy. Opt. Lett. 30, 468–470.
Martin, J.P., Logsdon, N., 1987. Oxygen radicals mediate cell inactivation by acridine dyes, fluorescein, and lucifer yellow CH. Photochem. Photobiol. 46, 45–53.
Martinez, V.A., Besseling, R., Croze, O.A., Tailleur, J., Reufer, M., Schwarz-Linek, J., Wilson, L.G., Bees, M.A., Poon, W.C., 2012. Differential dynamic microscopy: a high-throughput method for characterizing the motility of microorganisms. Biophys. J. 103, 1637–1647.
Maslov, I., Bogorodskiy, A., Mishin, A., Okhrimenko, I., Gushchin, I., Kalenov, S., Dencher, N.A., Fahlke, C., Buldt, G., Gordeliy, V., Gensch, T., Borshchevskiy, V., 2018. Efficient non-cytotoxic fluorescent staining of halophiles. Sci. Rep. 8, 2549.
Meacock, O.J., Durham, W.M., 2022. Tracking bacteria at high density with FAST, the Feature-Assisted Segmenter/Tracker. https://www.biorxiv.org/content/10.1101/2021.11.26.470050v3.
Micó, V., García, J., Camacho, L., Zalevsky, Z., 2011. Quantitative phase imaging in microscopy using a spatial light modulator. In: Ferraro, P., Wax, A., Zalevsky, Z. (Eds.), Coherent Light Microscopy: Imaging and Quantitative Phase Analysis. Springer Berlin Heidelberg, Berlin, Heidelberg, pp. 145–167.
Miyata, M., Robinson, R.C., Uyeda, T.Q.P., Fukumori, Y., Fukushima, S.I., Haruta, S., Homma, M., Inaba, K., Ito, M., Kaito, C., Kato, K., Kenri, T., Kinosita, Y., Kojima, S., Minamino, T., Mori, H., Nakamura, S., Nakane, D., Nakayama, K., Nishiyama, M., Shibata, S., Shimabukuro, K., Tamakoshi, M., Taoka, A., Tashiro, Y., Tulum, I., Wada, H., Wakabayashi, K.I., 2020. Tree of motility – A proposed history of motility systems in the tree of life. Genes Cells 25, 6–21.

Myung, K.K., 2010. Principles and techniques of digital holographic microscopy. SPIE Rev. 1, 018005.
Nadeau, J.L., Bin Cho, Y., Kuhn, J., Liewer, K., 2016. Improved tracking and resolution of bacteria in holographic microscopy using dye and fluorescent protein labeling. Front. Chem. 4.
Najafi, J., Shaebani, M.R., John, T., Altegoer, F., Bange, G., Wagner, C., 2018. Flagellar number governs bacterial spreading and transport efficiency. Sci. Adv. 4, eaar6425.
Nan, B., Zusman, D.R., 2016. Novel mechanisms power bacterial gliding motility. Mol. Microbiol. 101, 186–193.
Newby, J.M., Schaefer, A.M., Lee, P.T., Forest, M.G., Lai, S.K., 2018. Convolutional neural networks automate detection for tracking of submicron-scale particles in 2D and 3D. Proc. Natl. Acad. Sci. U. S. A. 115, 9026–9031.
O'Connor, O.M., Alnahhas, R.N., Lugagne, J.B., Dunlop, M.J., 2022. DeLTA 2.0: A deep learning pipeline for quantifying single-cell spatial and temporal dynamics. PLoS Comput. Biol. 18, e1009797.
Pané, S., Puigmartí-Luis, J., Bergeles, C., Chen, X.-Z., Pellicer, E., Sort, J., Počepcová, V., Ferreira, A., Nelson, B.J., 2019. Imaging technologies for biomedical micro- and nanoswimmers. Adv. Mat. Technol. 4, 1800575.
Peng, G., Caojin, Y., 2022. Resolution enhancement of digital holographic microscopy via synthetic aperture: a review. Light Adv. Manuf. 3, 105–120.
Piedrahita-Quintero, P., Castaneda, R., Garcia-Sucerquia, J., 2015. Numerical wave propagation in ImageJ. Appl. Opt. 54, 6410–6415.
Piepenbrink, K.H., Lillehoj, E., Harding, C.M., Labonte, J.W., Zuo, X., Rapp, C.A., Munson, R.S., Goldblum, S.E., Feldman, M.F., Gray, J.J., Sundberg, E.J., 2016. Structural diversity in the type IV Pili of multidrug-resistant Acinetobacter. J. Biol. Chem. 291, 22924–22935.
Pohl, O., Hintsche, M., Alirezaeizanjani, Z., Seyrich, M., Beta, C., Stark, H., 2017. Inferring the chemotactic strategy of *P. putida* and *E. coli* using modified Kramers-Moyal coefficients. PLoS Comput. Biol. 13, e1005329.
Pollitt, E.J.G., Diggle, S.P., 2017. Defining motility in the Staphylococci. Cell. Mol. Life Sci. 74, 2943–2958.
Rappaz, B., Marquet, P., Cuche, E., Emery, Y., Depeursinge, C., Magistretti, P., 2005. Measurement of the integral refractive index and dynamic cell morphometry of living cells with digital holographic microscopy. Opt. Express 13, 9361–9373.
Rastadter, K., Tramontano, A., Wurm, D.J., Spadiut, O., Quehenberger, J., 2022. Flow cytometry-based viability staining: an at-line tool for bioprocess monitoring of *Sulfolobus acidocaldarius*. AMB Express 12, 107.
Rosser, G., Fletcher, A.G., Wilkinson, D.A., de Beyer, J.A., Yates, C.A., Armitage, J.P., Maini, P.K., Baker, R.E., 2013. Novel methods for analysing bacterial tracks reveal persistence in *Rhodobacter sphaeroides*. PLoS Comput. Biol. 9, e1003276.
Rouzie, D., Lindensmith, C.N., Jay, 2021. Microscopic object classification through passive motion observations with holographic microscopy. Life 11.
Ruffner, D.B., Cheong, F.C., Blusewicz, J.M., Philips, L.A., 2018. Lifting degeneracy in holographic characterization of colloidal particles using multi-color imaging. Opt. Express 26, 13239–13251.
Schindelin, J., Arganda-Carreras, I., Frise, E., Kaynig, V., Longair, M., Pietzsch, T., Preibisch, S., Rueden, C., Saalfeld, S., Schmid, B., Tinevez, J.Y., White, D.J., Hartenstein, V., Eliceiri, K., Tomancak, P., Cardona, A., 2012. Fiji: an open-source platform for biological-image analysis. Nat. Methods 9, 676–682.
Schnars, U., Jüptner, W.P., 2002. Digital recording and numerical reconstruction of holograms. Meas. Sci. Technol. 13, R85.
Schneider, W.R., Doetsch, R.N., 1974. Velocity measurements of motile bacteria by use of a videotape recording technique. Appl. Microbiol. 27, 283–284.
Schuech, R., Hoehfurtner, T., Smith, D.J., Humphries, S., 2019. Motile curved bacteria are Pareto-optimal. Proc. Natl. Acad. Sci. 116, 14440–14447.
Sirico, D.G., Miccio, L., Wang, Z., Memmolo, P., Xiao, W., Che, L., Xin, L., Pan, F., Ferraro, P., 2022. Compensation of aberrations in holographic microscopes: main strategies and applications. Appl. Phys. B Lasers Opt. 128, 78.
Stocker, R., 2011a. Reverse and flick: Hybrid locomotion in bacteria. Proc. Natl. Acad. Sci. 108, 2635–2636.
Stocker, R., 2011b. Reverse and flick: Hybrid locomotion in bacteria. Proc. Natl. Acad. Sci. U. S. A. 108, 2635–2636.
Swedlow, J.R., 2013. Quantitative fluorescence microscopy and image deconvolution. Methods Cell Biol. 114, 407–426.
Tahara, Y., Yamazaki, M., Sukigara, H., Motohashi, H., Sasaki, H., Miyakawa, H., Haraguchi, A., Ikeda, Y., Fukuda, S., Shibata, S., 2018. Gut microbiota-derived short chain fatty acids induce circadian clock entrainment in mouse peripheral tissue. Sci. Rep. 8.
Taute, K.M., Gude, S., Tans, S.J., Shimizu, T.S., 2015. High-throughput 3D tracking of bacteria on a standard phase contrast microscope. Nat. Commun. 6.
Turner, L., Ping, L., Neubauer, M., Berg, H.C., 2016. Visualizing flagella while tracking bacteria. Biophys. J. 111, 630–639.
Wainwright, M., Phoenix, D.A., Marland, J., Wareing, D.R., Bolton, F.J., 1997. In-vitro photobactericidal activity of aminoacridines. J. Antimicrob. Chemother. 40, 587–589.
Wang, A., Dimiduk, T.G., Fung, J., Razavi, S., Kretzschmar, I., Chaudhary, K., Manoharan, V.N., 2014. Using the discrete dipole approximation and holographic microscopy to measure rotational dynamics of non-spherical colloidal particles. J. Quant. Spectrosc. Radiat. Transf. 146, 499–509.
Wang, A., Garmann, R.F., Manoharan, V.N., 2016. Tracking E-coli runs and tumbles with scattering solutions and digital holographic microscopy. Opt. Express 24, 23719–23725.
Wang, H., Lyu, M., Situ, G., 2018. eHoloNet: a learning-based end-to-end approach for in-line digital holographic reconstruction. Opt. Express 26, 22603–22614.
Waterbury, J.B., Willey, J.M., Franks, D.G., Valois, F.W., Watson, S.W., 1985. A cyanobacterium capable of swimming motility. Science. 230, 74–76.
Waters, J.C., Wittmann, T., 2014. Chapter 1 - Concepts in quantitative fluorescence microscopy. In: Waters, J.C., Wittman, T. (Eds.), Methods in Cell Biology, vol. 123. Academic Press, pp. 1–18.
Wilson, L.G., Martinez, V.A., Schwarz-Linek, J., Tailleur, J., Bryant, G., Pusey, P.N., Poon, W.C., 2011. Differential dynamic microscopy of bacterial motility. Phys. Rev. Lett. 106, 018101.
Wyatt, P.J., 1970. Cell wall thickness, size distribution, refractive index ratio and dry weight content of living bacteria (*Staphylococcus aureus*). Nature. 226, 277–279.
Xiao, Y., Jisoo, H., Changgeng, L., Myung, K.K., 2014. Review of digital holographic microscopy for three-dimensional profiling and tracking. Opt. Eng. 53, 112306.
Xie, J., Khan, S., Shah, M., 2008. Automatic tracking of *Escherichia Coli* bacteria. In: Metaxas, D., Axel, L., Fichtinger, G., Székely, G. (Eds.), Medical Image Computing and Computer-Assisted Intervention – MICCAI 2008. Springer Berlin Heidelberg, Berlin, Heidelberg, pp. 824–832.
Yang, T., Zheng, T., Shang, Z., Wang, X., Lv, X., Yuan, J., Zeng, S., 2015. Rapid imaging of large tissues using high-resolution stage-scanning microscopy. Biomed. Opt. Exp. 6, 1867–1875.
Yuan, K., Jurado-Sánchez, B., Escarpa, A., 2021. Dual-propelled lanbiotic based janus micromotors for selective inactivation of bacterial biofilms. Angew. Chem. Int. Ed. 60, 4915–4924.
Zhang, Y., Pedrini, G., Osten, W., Tiziani, H.J., 2003. Whole optical wave field reconstruction from double or multi in-line holograms by phase retrieval algorithm. Opt. Express 11, 3234–3241.
Zhang, Y.-G., Wu, S., Xia, Y., Sun, J., 2014. Salmonella -infected crypt-derived intestinal organoid culture system for host-bacterial interactions. Phys. Rep. 2, e12147.
Zhang, J., Zuo, C., Sun, J., Feng, S., Zhang, L., Fan, Y., Hu, Y., Kong, F., Chen, Q., Zhang, Y., Chen, D., Tao, T., Lin, F., Yang, Y., Tian, C., 2015. Software design of a digital holographic microscope based on MFC, multi-document and multi-thread.
Zhang, H., Stangner, T., Wiklund, K., Rodriguez, A., Andersson, M., 2017. UmUTracker: a versatile MATLAB program for automated particle tracking of 2D light microscopy or 3D digital holography data. Comput. Phys. Commun. 219, 390–399.
Zhu, T., Guo, Y., Zhang, Y., Lu, Z., Lin, X., Fang, L., Wu, J., Dai, Q., 2022. Noise-robust phase-space deconvolution for light-field microscopy. J. Biomed. Opt. 27.
Ziegler, A., Schock-Kusch, D., Bopp, D., Dounia, S., Radle, M., Stahl, U., 2015. Single bacteria movement tracking by online microscopy–a proof of concept study. PLoS One 10, e0122531.